Numerical Simulations of Combustion in SI Engines : Comparison of the Fractal Flame Model to the Coherent Flame Model

X.Zhao, R.D.Matthews and J.L.Ellzey

Mechanical Engineering Department
The University of Texas at Austin
Austin, Texas 78712-1063
USA

ABSTRACT

Turbulent combustion processes in two SI engines were simulated via multi-dimensional calculations using two flamelet models: the Coherent Flame Model (CFM) and the Fractal Flame Model (FFM). Predictions are compared to available experimental results. It is demonstrated that the FFM is more effective than the CFM in modeling premixed flame propagation in SI engines.

INTRODUCTION

For conventional spark ignition (SI) engines, experimental evidence indicates that the dominant effect of turbulence is to wrinkle the flame, resulting in a very thin but highly wrinkled flame involving a spectrum of length scales ranging from ~10 μm to ~100 mm. Thus, direct numerical simulation of SI engine combustion processes is practically impossible in the near future because of the computer time and memory requirements for calculations with grid sizes of the order of 10 μm [1,2]. The current alternative approach to the solution of reacting turbulent flows is to model the turbulence and combustion. That is, instead of solving the instantaneous Navier Stokes equations for the reacting turbulent flow, the primary variables are broken into two parts: an average part, or mean, and a fluctuating part representing instantaneous deviations from the mean. A set of statistically averaged governing equations are then formulated and solved in conjunction with sub-models for the turbulence and combustion, as needed to close the set of averaged equations.

Some recent combustion models are based upon the flamelet assumption, for which the chemistry is assumed to be fast enough so that the burned gases and the unburned gases can be considered as separated by very thin flamelets, and the local structure of the flamelets is the same as, or sufficiently close to, that of a laminar flame. In other words, it is assumed that the dominant effect of turbulence on the flame is to wrinkle the flame surface while the inner flame structure is not significantly altered by the turbulent flow field. The significance of the flamelet assumption is that it decouples the chemistry from the turbulence and, thereby, reduces the problem of modeling premixed turbulent combustion to the description of flame surfaces. Under the flamelet assumption, the mean reaction rate or mass burning rate can be evaluated as

$$\overline{\dot{\omega}} = A_f \cdot S_L \cdot \rho_u \qquad (1)$$

where the flame surface area is determined on a unit computational volume basis and the other terms are defined in the nomenclature section.

The flamelet assumption is valid in most, or perhaps even all, cases for SI engines. At the present time, perhaps the most widely recognized flamelet model is the Coherent Flame Model (CFM) [3-5]. The CFM uses a balance equation to describe flame surface production, destruction, diffusion, and advection in a reacting turbulent flow. However, the CFM requires the solution of an additional PDE for the flame surface area. We examined the CFM in a previous study [6]. In the present paper, we examine a different flamelet model, the Fractal Flame Model (FFM), which is based upon use of fractal geometry to quantify the effects of wrinkling on the flame surface area. Three-dimensional combustion simulations are performed on two different engines, and the results are compared to available experimental data.

THE FLAMELET MODELS

As discussed in the previous section, both the CFM and the FFM are based upon the flamelet assumption. Because of the flamelet assumption, the problem of modeling turbulent combustion is reduced to the description of flame surface area. The CFM and the FFM differ from each other in the way the flame surface areas are quantified, as described below.

THE COHERENT FLAME MODEL uses a balance equation for the flame surface area to describe the transport of the flame surface by the turbulent flow field and the physical mechanisms which produce and destroy the reactive surface. It was introduced and named the "Coherent Flame Model" by Marble and Broadwell in their analysis of turbulent diffusion flames [7]. In premixed turbulent combustion, this model is only applicable in the flamelet regime. The balance equation for the flame surface area is generally written as:

{ transport } = { turbulent diffusion } + { production } - { destruction }

One can derive the balance equation for flame surface area density starting from the basic transport equation for an averaged material surface area per unit volume $\overline{\Sigma}$:

$$\frac{\partial \overline{\Sigma}}{\partial t} + \frac{\partial}{\partial x_i}(\overline{V}_i \cdot \overline{\Sigma}) = \overline{-(n_i n_j s_{ij} - s_{kk}) \cdot \Sigma} + \frac{\partial}{\partial x_i}\overline{(V_i' \Sigma')} \qquad (2)$$

where

$$s_{ij} = \frac{1}{2}\left(\frac{\partial V_i}{\partial x_j} + \frac{\partial V_j}{\partial x_i}\right) \qquad (3)$$

designates the rate of strain tensor and n_i are the components of the normal to Σ.

In Eq. (2), the first term on the LHS is the rate of change of the material surface density, the second term on the LHS is the advection of the material surface by the bulk flow, and the first term on the RHS represents the material surface production by the stretch of turbulent eddies. The last term on the RHS accounts for the turbulent diffusion of the material surface.

At this point it is necessary to make use of the closure assumptions. A standard expression for the turbulent flux term is

$$-\overline{(V_i' \Sigma')} = D_t \frac{\partial \overline{\Sigma}}{\partial x_i} \qquad (4)$$

where D_t is the turbulent diffusivity.

The production term (the first term on the right hand side of Eq. (2)) can be modeled as [8]:

$$\overline{-(n_i n_j s_{ij} - s_{kk})\cdot\Sigma} = \alpha_{UT}\,\Gamma_{\bar{k}}\,\varepsilon_s\overline{\Sigma}_f\left(Re_L\frac{\delta_L}{L}\right)^{2(\gamma-1)} \qquad (5)$$

where

α_{UT}: model constant,
ε_S: mean strain rate,
Re_L: turbulent Reynolds number,
δ_L: laminar flame thickness,
L: integral length scale,
γ=0.7 and

$$\Gamma_{\bar{k}} = f\left(\frac{L}{\delta_L},\ \frac{u'}{S_L}\right)$$

Relations for calculating $\Gamma_{\bar{k}}$ were obtained from a recent study on the stretching and quenching of flamelets in premixed turbulent combustion [9]. This parameter accounts for the flame stretch by all sizes of eddies.

Since a flame surface is not a material surface, the balance equation for the flame surface density Σ_f is modeled by adding a destruction term to the balance equation for Σ. This destruction term describes the reduction of flame area by consumption of the reactants separating adjacent flame surfaces. For premixed flames, the rate of annihilation of flame surface may be modeled as:

$$\frac{1}{\overline{\Sigma}_f}\frac{\partial\overline{\Sigma}_f}{\partial t} = -\beta\frac{\overline{\dot{m}}}{\overline{m}_f} \qquad (6)$$

where β is another constant in the Coherent Flame Model and

$$\overline{\dot{m}} = \rho_u\cdot S_L\cdot\overline{A}_f$$

$$\overline{m}_f = \rho\cdot\overline{Y}_f\cdot V$$

The balance equation for the mean flame surface density may be finally written as:

$$\frac{\partial\overline{\Sigma}_f}{\partial t} + \frac{\partial}{\partial x_i}(\overline{V}_i\cdot\overline{\Sigma}_f) = \alpha_{UT}\,\Gamma_{\bar{k}}\,\varepsilon_s\overline{\Sigma}_f\left(Re_L\frac{\delta_L}{L}\right)^{2(\gamma-1)} + \frac{\partial}{\partial x_i}\left(D_t\frac{\partial\overline{\Sigma}_f}{\partial x_i}\right) - \beta\frac{\rho_u S_L\overline{\Sigma}_f^{\,2}}{\rho\overline{Y}_f} \qquad (7)$$

The Coherent Flame Model (CFM) has been extended and applied most recently to modeling combustion in SI engines [3,4,6]. Compared to our prior work [6] and to the other prior CFM applications to SI engines [3,4], the present version of the CFM is different in the formulation of flame surface area production. Also, a flame stretch model and different models for kernel formation and early flame growth were included. Details of these improvements to CFM are given in [8].

THE FRACTAL FLAME MODEL uses the concepts of fractal geometry to account for wrinkling of the flame surface by the turbulence and also accounts for the flame strain imposed by the turbulent eddies. Gouldin was the first to apply the concepts of fractal geometry to the study of turbulent flames [10]. He pointed out that prior models of wrinkled laminar flames were not successful in part due to the fact that only one scale of surface wrinkling was considered. Experimental studies of flames in SI engines [11,12] have revealed that the flame surface exhibits fractal characteristics and therefore can be described using fractal geometry. Assuming that turbulence results in homogeneous and isotropic wrinkling, the surface area A_f of a wrinkled flame front in the flamelet regime can be calculated as

$$A_f = A_i = A_o\left(\frac{\varepsilon_i}{\varepsilon_o}\right)^{2-D} \qquad (8)$$

where ε_i is the inner cutoff (the minimum flame wrinkling scale), ε_O is the outer cutoff (the maximum flame wrinkling scale), A_i is the flame surface area as measured using length scale ε_i, A_O is the flame surface area as measured using length scale ε_O, and D is the fractal dimension of the wrinkled flame surface (a quantitative measure of the distribution of flame wrinkling scales between the extremes of ε_i and ε_O).

In a previous study [8,14], we analyzed the fractal burning rate expression proposed by Gouldin and coworkers [13] for multi-dimensional simulations. In their work the outer cutoff, ε_O, was taken as the integral length scale, L, and the inner cutoff, ε_i, as the Kolmogorov length scale divided by a factor f, i. e., $\varepsilon_i=\eta/f$. The term (η/f) recognizes that the minimum flame wrinkling scale is larger than the smallest turbulent eddy size due to the smoothing effect of the local flame propagation process on the small scale wrinkles. However, we found [14] that use of the relationship posed for factor f [13] produced results that were too insensitive to turbulence intensity (engine speed). Gülder [15] proposed another model for $\varepsilon_i/\varepsilon_o$, which we [8] also found to have both strenghts and difficulties. In our development of the FFM, we incorporated the best features of both Gouldin's and Gülder's models. Also included in the FFM is a model accounting for the effect of flame strain. The FFM burning rate equation is:

$$\overline{\dot{\omega}} = C_F'\,\rho_u\,S_L\left(\frac{\delta_L}{L}\right)^{1/2}\left(1 - A'\left(\frac{\delta_L}{L}\right)^2 Re_L^{3/2}\right)\left(\frac{Re_L^{(3D-4)/4}}{L}\right)\overline{c}(1-\overline{c}) \qquad (9)$$

where

$$\overline{c} = \frac{\overline{Y}_{fu} - \overline{Y}_f}{\overline{Y}_{fu} - \overline{Y}_{fb}}$$

A': constant in the flame stretch submodel (=0.1), and

C_F': model constant.

A detailed discussion of the derivation of Eq. (9) is given in reference [8].

Gouldin et al. [13] did not suggest a model for the fractal dimension while Gülder assumed a constant fractal dimension. In the present study, a new correlation was obtained by curve-fitting the experimental measurements (see Fig. 1) conducted previously by North and Santavicca [16] using the turbulent Reynolds number $Re_L = u' L/\nu = (u'/S_L)(L/\delta_L)$ as the independent variable, instead of the more common dependence upon u'/S_L only:

$$D = 2.0\frac{200}{Re_L + 200} + 2.35\frac{Re_L}{Re_L + 200} \qquad (10)$$

Unlike the CFM, the FFM does not require the solution of an additional transport equation for flame surface area density. The gases in the engine combustion chamber are divided into two species: burned and unburned. To simplify this initial examination of the FFM, the composition of the burned gas is assumed to be that resulting from complete combustion.

KERNEL FORMATION AND EARLY FLAME GROWTH - The combustion process in SI engines may be generally divided into four processes: kernel formation, early flame growth, fully developed turbulent combustion, and last

10% burned. The CFM and FFM as posed above are not suitable for the first two stages. The techniques used to simulate these two stages are discussed below.

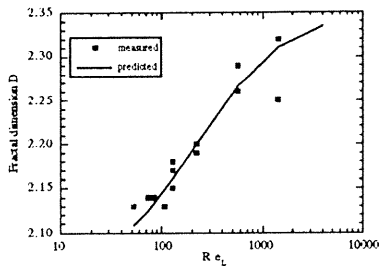

Fig. 1 Variation of fractal dimension with the turbulent Reynolds number

According to Herweg and Maly [17], kernel formation is dominated by the properties of the ignition system, not by flow or combustion effects. It is not until the flame kernel has reached a certain radius that the turbulent eddies and burning begin to have significant effects. Modeling the spark discharge processes (breakdown, arc, and glow) is usually difficult and requires significant computer time. Since our primary interest is in flame propagation rather than ignition, we simulated kernel formation as a period of 0.2 ms during which the flame grows to a radius of 1 mm. Herweg and Maly [17] showed that these two parameters are relatively insensitive to ignition system type, equivalence ratio, spark location, and engine speed.

During early flame growth, the flame is smaller than many of the eddy sizes. Thus, use of the integral scale to represent the maximum flame wrinkling scale is not appropriate during this stage. Rather, we assume that the flame grows spherically as a wrinkled laminar flame and use the instantaneous flame radius as the maximum wrinkling scale. Based on a mass balance and fractal geometry, a relation for the flame radius R_f can be derived as:

$$R_f = \left[R_{f0}^{3-D} + (3-D) S_L \left(\frac{T_b}{T_u}\right)\left(\frac{1}{\eta}\right)^{D-2} (t - t_{ign.}) \right]^{\frac{1}{3-D}} \quad (11)$$

where R_{f0} is the flame kernel radius at the end of the kernel formation process (1 mm), T_b and T_u are the temperatures of the burned and unburned gases, and t_{ign} is the time at ignition. The instantaneous flame surface area density that is used during early flame growth is calculated as:

$$\overline{\Sigma}_f = \frac{4\pi R_f^2}{Vol_{cell}} \left(\frac{R_f}{\eta}\right)^{D-2} \quad (12)$$

where Vol_{cell} is the volume of the computational cell that contains the ignition site.

The kernel formation and early flame growth models given above were used in all CFM and FFM calculations. The conventional CFM and FFM models are used during fully developed turbulent combustion, which begins when the flame radius equals the integral length scale.

COMBUSTION SIMULATIONS

Three-dimensional simulations of SI engine combustion processes were performed on a CRAY Y-MP using the KIVA-II code [18] as modified to incorporate the CFM and FFM to determine the mass burning rate. For turbulent reacting flows, KIVA-II uses the classical approach to turbulent problems, that is, the averaged governing equations are solved in conjunction with turbulence and combustion modeling. The k-ε model incorporated in KIVA-II for simulating the turbulence was used without modification.

The two engines simulated are the single cylinder research engine at Sandia National Laboratory (the Sandia engine) and the GSM-IFP engine at Institut Francais du Petrole (the IFP engine). A detailed discussion of these two engines is presented in the original references [19,20]. Major engine parameters are provided in Table 1 and the combustion chamber geometries are illustrated in Fig. 1. The engine operating conditions simulated are provided in Table 2. Both engines were run on propane-air mixtures.

The unstretched laminar flame speed was determined using the correlation of Metghalchi and Keck [21]. The laminar flame thickness δ_L was calculated based upon the relation: $\delta_L = \nu / S_L$. A cylindrical grid of 20 x 36 x 8 (radial x azimuthal x axial) was used in the calculations with ignition at the cylinder wall. For the cases with central ignition, a cylindrical grid of 20 x 1 x 8 (radial x azimuthal x axial) was used because our previous three-dimensional calculations in cases with central ignition revealed that such flame propagation processes are very close to axisymmetric. The computer time requirements are reduced significantly by changing the central ignition calculations from 3-D to 2-D.

For both engines, the law-of-the-wall boundary conditions incorporated in KIVA-II were used and initial conditions were obtained based on experimental measurements (see Table 3). The mixture temperatures for the IFP engine were obtained from a thermodynamic analysis by Baritaud. For the Sandia engine, a mixture temperature at 20 CA° BTDC was assumed. It is believed that adjustments to the model constants may be used to compensate for errors in this assumption.

The model constants (α_{UT} and β in the CFM, C_F' in the FFM) were determined by matching the predicted pressure histories for the baseline case for each engine with the experimental results.

Table 1 Engine Specifications

Engine	IFP	Sandia
Displacement	476 cc	462 cc
Bore	86 mm	76.2 mm
Stroke	82 mm	82.55 mm
Rod to half stroke ratio	3.341	4.918
Clearance at TDC	15.4 mm	18.76 mm
Compression ratio	6.2	5.4

Predicted burned mass fraction histories using both the CFM and the FFM are compared to the experimental results for the IFP engine in Fig. 3. With variations in spark timing (Case S12E), speed (Case S6IJ), equivalence ratio (Case S12G), and load (Case S12B), predictions using the FFM agree with the experimental results very well except for the last stage of combustion, for which a model is not yet available. Calculations using the CFM are not as good as those of the FFM, especially for the lean case (S12G).

Results for the Sandia engine are shown in Fig. 4. Since the burned mass fraction data were not available for this engine, we compared the predicted engine cylinder pressures to the experimental results. The case with central ignition at 1200 rpm was chosen as the baseline case. For the cases with wall ignition, both the CFM and the FFM over-predict the rate of cylinder pressure rise significantly. Both models appear to

require a longer ignition delay in these sidewall ignition cases. However, the cause of this overprediction of burning rate might be associated with the cylindrical computational grid used in the calculations, not with the combustion models. With off-axis ignition, the flame not only propagates in the radial direction, but also in the azimuthal direction. By using the cylindrical grid, cell volumes are greater at larger radius than those at smaller radius because of the non uniformity of grid size in the azimuthal direction. This problem can be reduced by limiting the maximum grid size in the azimuthal direction.

There is another problem with the cylindrical grid, which also affects calculations with off-axis ignition. The central axis of the cylinder was treated mathematically as a boundary, while physically there is no such boundary in the middle of the combustion chamber. When the flame approaches the cylinder axis, it can only go around the axis instead of passing through it.

Table 2 Engine Operating Conditions

The Sandia Engine				The IFP engine					
rpm	ϕ	Spark	Spk Place	Test	rpm	ϕ	Vol.Eff.	Flow	Timing
1200	1	7 BTDC	Center	S12E	1200	0.9	0.5	Swirl	35 BTDC
600	1	3 BTDC	Center	S12FA	1200	0.9	0.5	Swirl	25 BTDC
1200	1	15 BTDC	R=3.81 cm	S12G	1200	0.7	0.5	Swirl	25 BTDC
600	1	11 BTDC	R=3.81 cm	S6IJ	600	0.9	0.5	Swirl	25 BTDC
1200	1	11 BTDC	R=2.86 cm	S12B	1200	0.9	0.9	Swirl	25 BTDC

Table 3 Initial conditions used in the engine simulations

The IFP Engine						The Sandia Engine					
Test	u' (m/s)	T (K)	p (kPa)	T_{wall} (K)	CA^{o} BTDC	Test	u' (m/s)	T (K)	p (kPa)	T_{wall} (K)	CA^{o} BTDC
S12G	2.5	605	354	325	34.8	1200 rpm, c*	7.00	670	722	350	20
S6IJ	1.5	642	375	325	34.8	600 rpm, c	2.60	670	707	350	20
S12E	2.5	570	272	325	44.8	1200 rpm, w*	7.00	670	728	350	20
S12FA	2.5	624	365	325	34.8	600 rpm, w	2.60	670	717	350	20
S12B	2.5	584	500	325	44.8	1200 rpm, s*	7.00	670	721	350	20

* - c=central ignition, s=3/4 radius ignition, w=ignition at wall

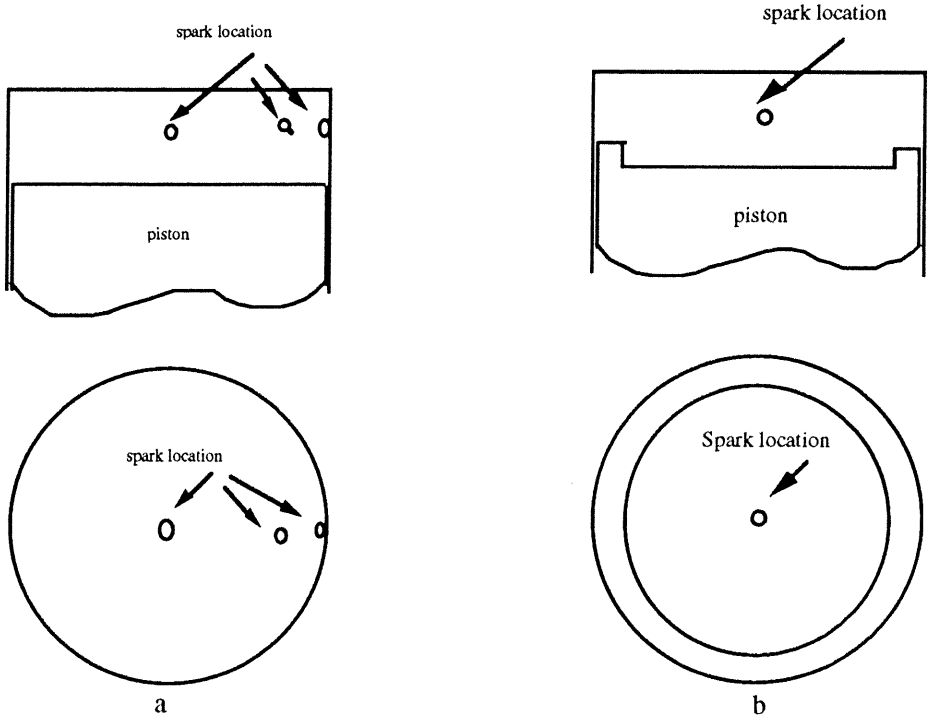

Fig.2 Schematic of the engine combustion chamber geometry
(a: The Sandia Engine; b: The IFP Engine)

Flame propagation contours with wall ignition at 1200 rpm for the Sandia engine via the CFM and the FFM are represented in the density contour plots of Fig. 5. The density contour plots indicate that reactions are occurring in a large (~7 mm thick) region in the combustion chamber. Our results do not indicate that the flame sheet is thick but rather that the

thin flame surface is highly convoluted and covers many computational cells.

SUMMARY AND CONCLUSIONS

Flame propagation in two research-type SI engines was simulated via multi-dimension calculations using two flamelet models: the Coherent Flame Model and the Fractal Flame Model. Both models were modified compared to the forms originally developed. New submodels have been used for the kernel formation and early flame growth processes. The FFM is more accurate for all cases examined, does not require solution of an additional differential equation, and has only one adjustable constant which appears to be only weakly engine-dependent (however, the present results also indicate that one of the two CFM constants is universal). More study is needed for cases with off-axis ignition. Although additional improvements to the CFM are expected, we believe that the present results indicate the merit of use of fractal geometry for quantifying the effects of turbulence in wrinkling and straining the flame surface.

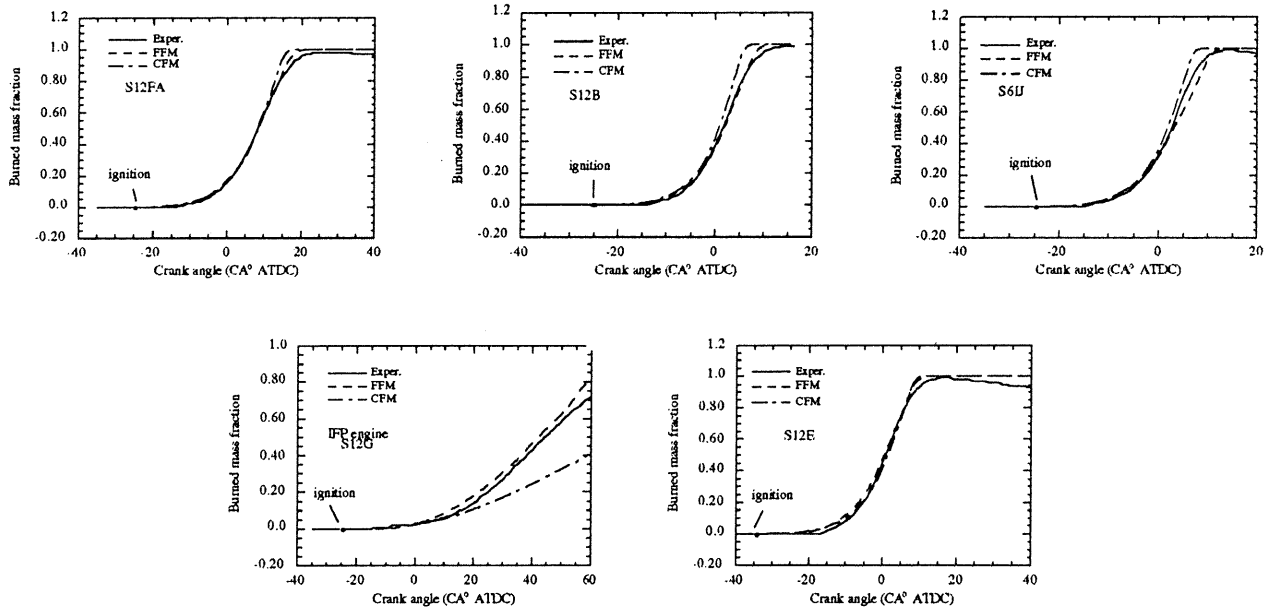

Fig. 3 Comparison of predicted engine burned mass fraction histories to experimental results (IFP engine, CFM model constants: α_{UT}=0.12, β=1.0, FFM model constant: C_F'=2.5)

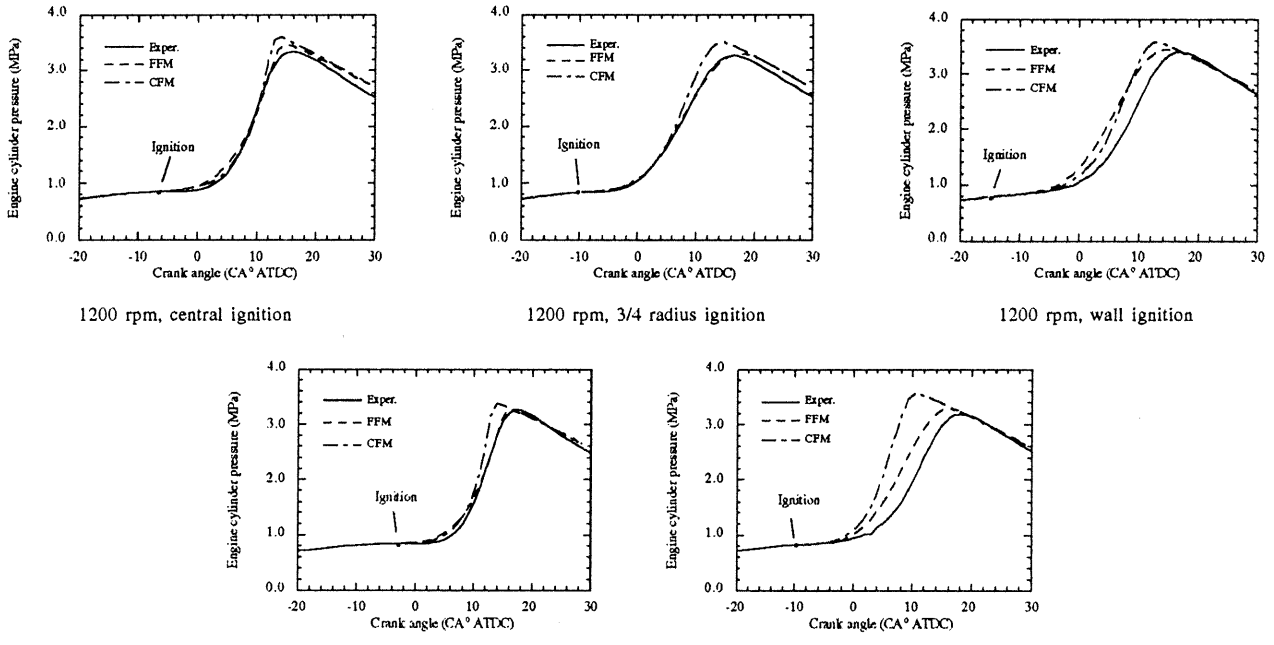

Fig. 4 Comparison of predicted engine cylinder pressure histories to experimental results (Sandia engine, CFM model constants: α_{UT}=0.16, β=1, FFM model constant: C_F'=2.7)

ACKNOWLEDGMENTS - Support for this work was provided by Cray Research, Inc., and the University of Texas System Center for High Performance Computing.

NOMENCLATURE

A_f Flame surface area

A_i	Flame surface area measured using length scale ε_i
A_o	Flame surface area measured using length scale ε_o
A'	FFM flame strain submodel constant (=0.1)
C_F'	FFM model constant
D	Fractal dimension
L	Integral length scale
Re_L	Turbulent Reynolds number (u' L/ν)
S_L	Unstretched laminar flame speed
u'	Turbulence intensity
Vol.Eff.	Volumetric efficiency
Y_f	Mass fraction of fuel in the mixture
Y_{fb}	Mass fraction of fuel in the burned region
Y_{fu}	Mass fraction of fuel in the unburned region
δ_L	Laminar flame thickness
ε	Rate of dissipation of turbulent kinetic energy
ε_s	Mean strain rate
ε_i	The minimum flame wrinkling scale
ε_o	The maximum flame wrinkling scale
ϕ	Equivalence ratio
η	Kolmogorov length scale
k	Turbulent kinetic energy
ν	Laminar kinematic viscosity
ρ	Density of mixture
ρ_u	Density of unburned gas
Σ	Material surface area per unit volume
Σ_f	Flame surface area per unit volume

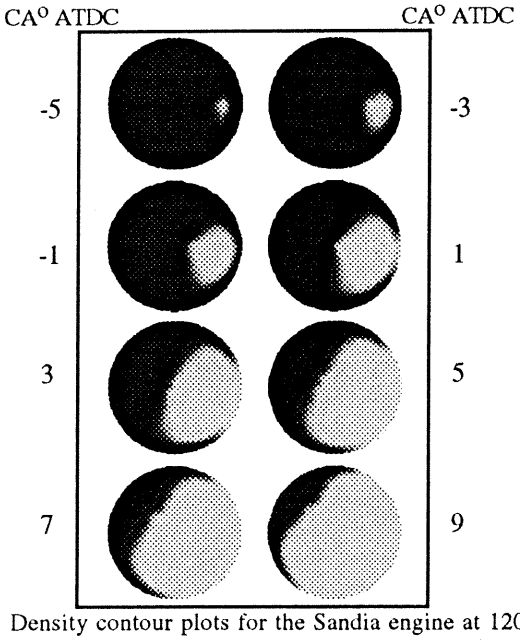

Fig. 5 Density contour plots for the Sandia engine at 1200 rpm with 3/4 radius ignition at the 3 O'Clock position and clockwise swirl using the FFM.

REFERENCES

[1] Pope, S.B., "Computations of Turbulent Combustion; Progress and Challenges", *23rd Symposium (International) on Combustion*, The Combustion Institute, Pittsburgh, pp. 591-612, 1990.

[2] Rutland, C.J., Ferziger, J.H., and El Tahry, S.H., "Full Numerical Simulations and Modeling of Turbulent Premixed Flames", *23rd Symposium (International) on Combustion*, The Combustion Institute, Pittsburgh, pp. 621-627, 1990.

[3] Cheng, W.K., and Diringer, J.A., "Numerical Modelling of SI Engine Combustion with a Flame Sheet Model", SAE Paper 910268, 1991.

[4] Boudier, P., Henriot, S., Poinsot, T., and Baritaud, T., "A Model For Turbulent Flame Ignition and Propagation in Spark Ignition Engines", *24th Symposium (International) on Combustion*, The Combustion Institute, Pittsburgh, in press, 1993.

[5] Duclos, J.M., Veynante, D., and Poinsot, T., "A Comparison of Flamelet Models for Premixed Turbulent Combustion", *Combustion and Flame*, **95**:101-117 (1993).

[6] Zhao, X., Matthews, R.D., and Ellzey, J.L., "Three-Dimensional Numerical Simulation of Flame Propagation in Spark Ignition Engines", SAE Paper 932713, 1993.

[7] Marble, F.E., and Broadwell, J.E., "The Coherent Flame Model for Turbulent Chemical Reactions", Project Squid Report TRW-9-PU, Purdue Univ., 1977.

[8] Zhao, X., "Multi-Dimensional Combustion Modeling of Premixed Turbulent Flames", Ph.D. Dissertation, University of Texas at Austin, May, 1994.

[9] Meneveau, C., and Poinsot, T., "Stretching and Quenching of Flamelets in Premixed Turbulent Combustion", *Combustion and Flame*, **86**:311-332, 1991.

[10] Gouldin, F.C., "An Application of Fractals to Modelling Premixed Turbulent Flames", *Combustion and Flame*, **68**:249-266 (1987).

[11] Mantzaras, J., Felton, P.G., and Bracco, F.V., "Fractals and Turbulent Premixed Engine Flames", *Combustion and Flame*, **77**:295-310 (1989).

[12] Hall, M.J., Dai, W., and Matthews, R.D., "Fractal Analysis of Turbulent Premixed Flame Images from SI Engines", SAE Paper 922242, 1992, accepted for the *Journal of Engines*, 1993.

[13] Gouldin, F.C., Bray, K.N.C., and Chen, J.Y., "Chemical Closure Model for Fractal Flamelets", *Combustion and Flame*, **77**:241-259 (1989).

[14] Zhao, X., Ellzey, J.L., and Matthews, R.D., "Calculation of the Combustion Process in a Square-piston SI Engine Using a Fractal Flame Model in the KIVA-II Code", presented at the 4th International KIVA Users Meeting, Detroit, February, 1994.

[15] Gülder, O.L., "Turbulent Premixed Combustion Modeling Using Fractal Geometry", *23th Symposium (International) on Combustion*, The Combustion Institute, Pittsburgh, pp. 835-842, 1990.

[16] North, G.L., and Santavicca, D.A.,"The Fractal Nature of Premixed Turbulent Flames", *Combustion Science and Technology*, **72**:215-232 (1990).

[17] Herweg, R., and Maly, R.R., "A Fundamental Model for Flame Kernel Formation in SI Engines", SAE Paper 922243, 1992.

[18] Amsden, A.A., O'Rourke, P.J., and Butler, T.D., "KIVA-II: A Computer Program for Chemically Reactive Flows with Spray", Los Alamos National Laboratory Report, LA-11560-MS, 1989.

[19] Baritaud, T.A., "Combustion and Fluid Dynamic Measurements in a Spark Ignition Engine: Effects of Thermochemistry and Velocity Field; Turbulent Flame Speeds", SAE Paper 892098, 1989.

[20] Witze, P.O., Martin, J.K. and Borgnakke, C., "Measurements and Predictions of the Precombustion Fluid Motion and Combustion Rates in a Spark Ignition Engine", SAE Paper 831697, 1983.

[21] Metghalchi, M. and Keck, J., "Laminar Burning Velocity of Propane Air Mixtures at High Temperature and Pressure", *Combustion and Flame*, **38**:143-154, 1982.